End-to-End Transmission Analysis of Simultaneous Wireless Information and Power Transfer Using Resonant Beam

Wen Fang , Hao Deng , Qingwen Liu , *Senior Member, IEEE*, Mingqing Liu , Mengyuan Xu,
Liuqing Yang , *Fellow, IEEE*, and Georgios B. Giannakis , *Fellow, IEEE*

Abstract—**Integrating the wireless power transfer (WPT) technology into the wireless communication system has been important for operational cost saving and power-hungry problem solving of electronic devices. In this paper, we propose a resonant beam simultaneous wireless information and power transfer (RB-SWIPT) system, which utilizes a gain medium and two retro-reflecting surfaces to enhance and retro-reflect energy, and allows devices to recharge their batteries and exchange information from the resonant beam wirelessly. To reveal the SWIPT mechanism and evaluate the SWIPT performance, we establish an analytical end-to-end (E2E) transmission model based on a modular approach and the electromagnetic field propagation. Then, the intra-cavity power intensity distribution, transmission loss, output power, and E2E efficiency can be obtained. The numerical evaluation illustrates that the exemplary RB-SWIPT system can provide about 4.20 W electric power and 12.41 bps/Hz spectral efficiency, and shorter transmission distance or larger retro-reflecting surface size can lead to higher E2E efficiency. The RB-SWIPT presents a new way for high-power, long-range WPT, and high-rate communication.**

Index Terms—**Simultaneous wireless information and power transfer, resonant beam, end-to-end transmission model, retro-reflecting surface.**

I. INTRODUCTION

WITH the rapid development of wireless communication technologies, the problem of energy consumption has become prominent [1]. The energy consumption of conventional communication devices relies heavily on rechargeable or replaceable batteries, which are expensive and the mobility of the device is limited. Recently, several renewable energy resources, such as solar, wind, have been integrated into communication

networks for power supply reference. However, the intermittent and unpredictable nature of these energy sources limits the application and quality-of-service (QoS) of energy harvesting (EH) technologies [2].

Wireless power transfer (WPT) is one of the EH technologies that overcome above limitations, which can provide enduring charging for communication devices. The prospect of integrating WPT with communication networks creates a need for technology that can transfer both information and energy simultaneously to devices. Therefore, the concept of simultaneous wireless information and power transfer (SWIPT) is first introduced in [3], and a capacity-energy function and a coding theorem are also defined. Developing green technologies and reducing the power consumption of devices are two of the eight major requirements for 5th generation mobile networks (5G) systems identified by industry and academia [4]. Thus, in the era of 5G, the SWIPT technology can be of fundamental importance for energy supply and information exchange among numerous devices [5], [6].

However, the existing long-range SWIPT technologies face short-range, low-power, unsafe and other challenges. For example, electromagnetic coupling SWIPT has the bottleneck of short transmission distance [7], radio-frequency (RF) and light-emitting diode (LED) lights based SWIPT face the challenge of low transmission power [8], [9], and laser-based SWIPT is difficult to achieve high power transmission safely [10].

Recently, Resonant Beam Charging (RBC), also known as Distribute Laser Charging (DLC), was proposed for high-power and long-range WPT, which relies on the spatially separated cavity to generate the resonant beam for transmitting energy over the air [11], [12]. The structure and characteristics of the RBC system were illustrated in [11], while the process of power transfer in the RBC system was studied in [12], [13]. [14] experimentally demonstrates that it is possible to realize long-range WPT in the RBC system. Furthermore, the RBC technology is identified as one of the innovations for power supply in 6th generation mobile networks (6G) [15]. Afterwards, [16] and [17] illustrate that the structure of the RBC system can also be used as a communication system to achieve high-rate, high-capacity communication.

Compared with the existing SWIPT technologies, as the energy carrier, the resonant beam can realize long-range, high-power, safe WPT, and high-rate communication. Thus, we

Fig. 1.   A typical application scenario of the RB-SWIPT system.

Fig. 2.   The RB-SWIPT system structure.

propose the resonant beam simultaneous wireless information and power transfer (RB-SWIPT) system based on the structure of RBC system, in which the resonant beam (intra-cavity laser) is the energy-information carrier. The input and output retro-reflectors are placed at the spatially separated transmitter and receiver and used to retro-reflect the resonant beam. Besides, the gain medium at the transmitter can amplify the resonant beam passing through it to provide energy. Fig. 1 illustrates a typical application scenario of the RB-SWIPT system. The end-device, e.g. mobile phones, intelligent speakers and intelligent lock systems, embedded with the SWIPT receiver can be charged and exchanged information wirelessly by the transmitter mounted on the ceiling. Thus, high throughput and energy sustainability can be realized for these devices.

In this paper, we first introduce the structure of RB-SWIPT system. Then, we adopt the electromagnetic field propagation and the modular approach to theoretically analyze the transmission model and accurately calculate transmission loss, output electric power, spectral efficiency, and end-to-end (E2E) efficiency. Finally, we evaluate energy and information transfer performance with different system parameters. The contributions of this paper include:

c1) We propose the resonant beam simultaneous wireless information and power transfer (RB-SWIPT) system, which can provide long-range, high-power WPT and high-rate communication simultaneously, and thus can support energy sustainability and high throughput for wireless devices.

c2) We establish an analytical end-to-end transmission model using modular approach and electromagnetic field propagation for the RB-SWIPT system. It can reveal the intra-cavity power intensity distribution, transmission loss, output power for energy-information transfer, and E2E efficiency numerically.

c3) The numerical evaluation illustrates that the exemplary RB-SWIPT system can provide about 4.20 W output electric power and 12.41 bps/Hz spectral efficiency.

In the rest of this paper, the RB-SWIPT system structure and E2E transmission model will be introduced in Section II. The RB-SWIPT model will be analyzed in Section III modularly. And then, the numerical evaluation of power intensity distribution, transmission loss, output beam power, output electric power, spectr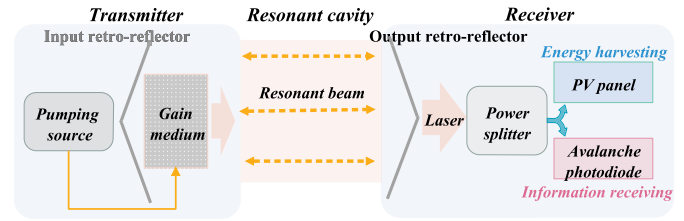al efficiency, and E2E efficiency will be described in Section IV. Finally, the paper will be concluded along with the future research in the RB-SWIPT system.

II. RB-SWIPT SYSTEM

The RB-SWIPT system is able to transfer power and information over a long-range owing to the spatially separated laser cavity structure. In this section, we first introduce the structure of the RB-SWIPT system. Then, the E2E SWIPT transmission model is presented summarily.

A. System Overview

The structure of the RB-SWITP system is depicted in Fig. 2. An RB-SWITP system consists of a transmitter and a receiver, which are spatially separated. The transmitter includes a retro-reflector with 100% reflectivity and a gain medium, and the receiver is comprised of a retro-reflector with partial reflectivity, a power splitter, a photovoltaic (PV) panel and an avalanche photodiode (APD). There exists resonant beam between the transmitter and receiver for energy and information transfer.

The energy transfer process in the RB-SWIPT system is as follows. i) In the transmitter, the pumping source provides the pumping electric power to stimulate the gain medium for generating the resonant beam. ii) The gain medium is stimulated to perform atomic transitions, and then form population inversions between the high and low energy levels, thereby pump out the resonant beam [18]. iii) The pump beam power transmits from the transmitter to the receiver over the air carried by resonant beam. iv) The output retro-reflector receives the beam power. Based on the reflectivity of output retro-reflector, part of beam passes through the retro-reflector forming the output beam, and the rest is reflected to the gain medium for amplification. For example, if the reflectivity of output retro-reflector is 90%, 10% of the received energy passes through the output retro-reflector to charge and communicate, and the remaining 90% is reflected to the transmitter. v) Finally, the power splitter distributes output power to PV panel converting into charging power and APD receiving information.

For the input and output retro-reflectors, regardless of the direction of the beam incident on the retro-reflector, the beam can be reflected towards the original direction. This property is called retro-reflection. The input/output retro-reflector can be Corner-Cube retro-reflector or cat's eye retro-reflector (CER) [19].

In this paper, we investigate the RB-SWIPT system with the cat's eye retro-reflector. As depicted in Fig. 3(a), a CER is generally composed of two hemispheres of different radii, which
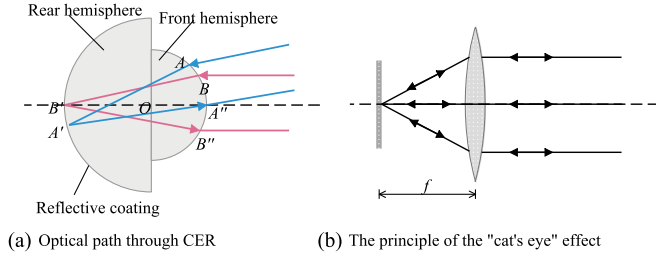
(a) Optical path through CER   (b) The principle of the "cat's eye" effect

Fig. 3.   The model of cat's eye retro-reflector.

are glued together centrifugally. Also, the front and rear hemispheres are centered at point O. To guarantee the retro-reflective property of CER, it must require the focal point of the image on the front hemisphere to fall on the surface of the rear hemisphere, and the surface of the rear hemisphere coated with a reflective film. For any near-axis beam, it will fall on the sphere of the rear hemisphere after the focus of the front hemisphere. Then, it will be reflected from the sphere of the rear hemisphere, which is equivalent to that a beam is emitted from the focal point of the rear hemisphere. The emitted beam is parallel to the incident beam, i.e. the CER is retro-reflective [20].

In Fig. 3(a), the two rays are incident from points A and B, reflected by points A' and B', and then refracted from points A'' and B'' respectively. This characteristic is also known as the "cat's-eye effect". As depicted in Fig. 3(b), the cat's eye effect can be simplified to a combined model of a lens and reflecting surface, where f is the focal length of the lens. If the focal length of the lens is small compared to the transmission distance, then the effect of focal length on beam transmission can be ignored, thereby the CER can be simplified as a retro-reflecting surface with equal reflecting aperture [21]. Thus, the resonant cavity of RB-SWIPT system can be equivalent to a Fabry-Pérot (FP) cavity [22].

B. End-to-End Transmission Model

As shown in Fig. 4, the E2E energy-information transfer process in the RB-SWIPT system can be divided into four steps: i) electric power pumping resonant beam, ii) resonant beam transmission, iii) receiving and reflecting resonant beam, and iv) energy harvesting and information receiving.

Among them, the electric power provides the energy for gain medium to stimulating out the resonant beam, so the efficiency of the "electric power pumping resonant beam" can be decided by the physical characteristic of the gain medium and the cross-sectional area of the pumping beam [14]. Then, the resonant beam transmits between the transmitter and the receiver. During the power transmission, due to the limited sizes of the input and output retro-reflectors and the existence of the deflection, diffraction, or other loss factors, there must be loss during the resonant beam transmission. Afterwards, the output retro-reflector receives the resonant beam. A portion of beam energy is reflected to the transmitter and the rest is devoted to energy and information transfer [23]. Finally, the output beam energy is converted into electric power and data by PV panel and APD respectively.

Based on the energy-information transfer process, we will establish a resonant beam transmission model based on electromagnetic field propagation for calculating the transmission loss accurately, and establish the end-to-end SWIPT model to study the energy and information transmission process modularly.

III. END-TO-END SWIPT MODEL

In the RB-SWIPT system, the energy-information transmission carrier is the resonant beam. To understand the transmission process, we establish the analytical E2E SWIPT model and analyze the transmission process modularly.

A. Electric Power Pumping Resonant Beam

The pump source provides the input electric power P_{in} to excite the beam out of the gain medium. The process of pumping resonant beam can be summarized as: i) input electric power P_{in} is converted into pumping optical power P_{gb}; ii) pumping optical power is absorbed by the gain medium and converted into the available pumping power (i.e. the power in the upper laser level) P_{av}; and, iii) P_{av} is used to realize population inversion and pump out the resonant beam.

The efficiency of the pumping process is given by the excitation efficiency η_{excit} [18],

$$\eta_{excit} = \frac{P_{av}}{P_{in}}. \tag{1}$$

For the homogeneously broadened lasers, the power in the upper laser level P_{av} is determined by its physical properties,

$$P_{av} = g_0 \ell A I_s, \tag{2}$$

where $g_0\ell$ is the small-signal gain, A is the cross-sectional area of the gain medium, and I_s is the saturation intensity, which is an attribute of the laser material. That is, I_s represents the peak incident light intensity that can be amplified by the gain medium, and it can be calculated by $I_s = h\upsilon/\sigma\tau$ for a four-level laser system, where $h\upsilon$ represents photon energy, σ is emission cross section for stimulated emission, and τ is spontaneous decay time of the upper laser level [18].

B. Resonant Beam Transmission

The resonant beam is a kind of electromagnetic wave. Thus, we analyze the resonant beam transmission between the transmitter and receiver based on the electromagnetic field propagation.

The Huygens-Kirchhoff principle in the optics shows that each position on the surface of the wave source can be regarded as a new wave source. From these positions (new wave sources), the wavelets are emitted. The field distribution at a position in space is the result of coherent superposition of these wavelets at that position [18], [24], [25]. The expression of this theory can be depicted as Fresnel-Kirchoff's diffraction integral:

$$u(x, y) = \frac{ik}{4\pi} \iint_S u(x', y') \frac{e^{-ik\rho}}{\rho}(1 + cos\theta)ds', \tag{3}$$

where $u(x', y')$ is the field distribution function of the wave source point (x', y') on the primary surface, and $u(x, y)$ is the
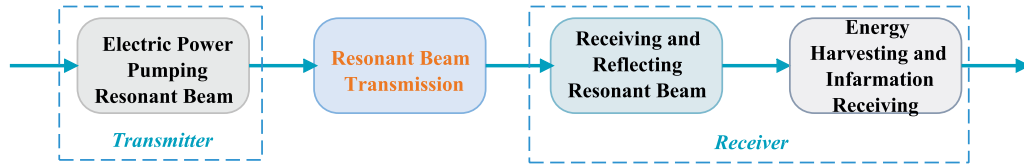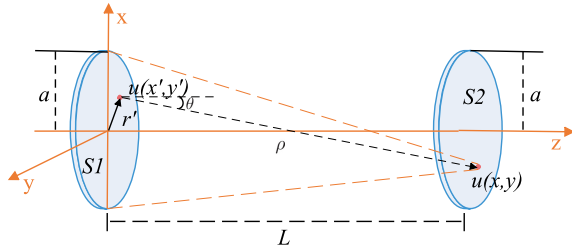
Fig. 4.   RB-SWIPT end-to-end transmission model.

Fig. 5.   Field analysis in the RB-SWIPT system.

(a) Beam transmission in the resonant cavity

(b) The formation of self-reproductive mode

Fig. 6.   Beam transmission in the resonant cavity (Self-reproductive mode, i.e. Fox-Li numerical iteration method).

field distribution function of the observation point (x, y). ρ is the distance from (x', y') to (x, y), and θ represents the angle between the direction determined by two the points $((x, y)$ and $(x', y'))$ and the unit normal to the wave source surface. In addition, i is the imaginary unit. k is the wave vector and can be calculated by

$$k = \frac{2\pi}{\lambda}, \qquad (4)$$

where λ represents the beam wavelength. ds' is the surface element at point (x', y') on the wave source surface.
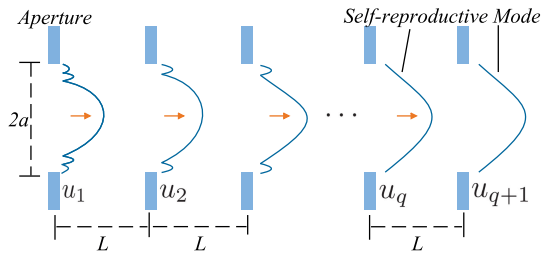
The beam propagation in the resonant cavity is actually the beam spatial diffraction process under the constraints of the retro-reflector sizes. Applying the Fresnel-Kirchoff's diffraction integral to the RB-SWIPT system shown in Fig. 5: the cavity length is L, the radii of the input and output retro-reflecting surfaces are a. r' represents the radius inside the surface (i.e. the distance between the center of the retro-reflecting surface $(0,0)$ and any point on the surface (x, y)). Besides, as illustrated in Fig. 5, $r' \leq a$. The optical axes of the surfaces $S1$ and $S2$ coincide. Besides, the direction of optical axis is taken as the z-axis, and the directions perpendicular to the optical axis are used as the x-axis and y-axis to establish a three-dimensional space rectangular coordinate system.

As shown in Fig. 5, the cavity length L is much greater than the retro-reflector diameter $2a$. The included angle between the propagation direction of paraxial rays and the optical axis is close to zero, so the distance between the positions on the two retro-reflectors can be approximately set as L. Therefore, the integral factor $(1 + cos\theta)/\rho$ in (3) can be set as $2/L$ approximately, and then it can be removed from the integral sign. And yet, after one propagation, the field distribution function $u_1(x', y')$ on surface $S1$ and the field distribution function $u_2(x, y)$ on surface $S2$ can be simplified as

$$u_2(x, y) = \frac{i}{\lambda L} \iint_{S1} u_1(x', y') e^{-ik\rho} ds'. \qquad (5)$$
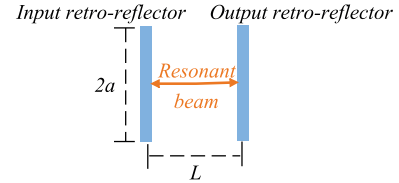
Then, after m propagations, the relationship between the field distribution function $u_m(x', y')$ on $S1$ and $u_{m+1}(x, y)$ on $S2$ also satisfies (5), that is

$$u_{m+1}(x, y) = \frac{i}{\lambda L} \iint_{S1} u_m(x', y') e^{-ik\rho} ds'. \qquad (6)$$

In the RB-SWIPT system, the resonant beam is reflected back and forth between two parallel retro-reflecting surfaces, as shown in Fig. 6(a). This is equivalent to a transmission line comprising a series of apertures as depicted in Fig. 6(b). Due to the limited geometry sizes of the retro-reflecting surfaces and the existence of loss factors such as absorption, scattering, and deflection, the wavefront of the resonant beam will distort after each aperture propagation, and part of the beam will deviate from the original direction. These deviated beams will be blocked the next time they pass through the aperture. In this way, the above transmission process is repeated in succession through the aperture.

Each time the resonant beam passes the aperture, its amplitude and phase change, and its energy is concentrated towards the optical axis. After multiple round trips, the amplitude distribution of the resonant beam remains essentially constant. Thus, a stable field distribution, which is called a self-reproductive mode, is formed. In the RB-SWIPT system, when the number of beam transmission m is sufficiently large, the field distribution on the retro-reflecting surface S1 is reproduced that on the

retro-reflecting surface S2:

$$u_{m+1} = \frac{1}{\tau} u_m, \tag{7}$$

that is, the field distribution u_{m+1} on the retro-reflecting surface S1 is identical to u_m on the retro-reflecting surface S2 except for a coordinate-independent complex constant factor τ representing the amplitude attenuation. This field whose amplitude distribution will no longer change is the resonant cavity mode, which can be expressed by the same function u,

$$u(x, y) = \tau \frac{i}{\lambda L} \iint_{S'} u(x', y') e^{-ik\rho} ds'. \tag{8}$$

Introducing an integral kernel associated with two retro-reflectors coordinate systems,

$$\Phi(x, y, x', y') = \frac{i}{\lambda L} e^{-ik\rho(x, y, x', y')}. \tag{9}$$

Then, (8) can be transformed into an integral eigenfunction with a complex constant eigenvalue,

$$u(x, y) = \tau \iint_{S'} \Phi(x, y, x', y') u(x', y') ds'. \tag{10}$$

A numerical iterative algorithm for calculating the integral eigenfunction of the resonant cavity is proposed by A. G. Fox and T. Li in 1960, which is called "Fox-Li" numerical iteration method [26]. The realization of the "Fox-Li" numerical iteration method relies on the fact that: the beam transmission in the resonant cavity can be simulated by the integral eigenfunction of the resonant cavity. As depicted in Fig. 6(b), during the resonant beam transmits between the input and output retro-reflecting surfaces, each time the integral is calculated, it's equivalent to one beam transmission process in the cavity. The result of the last calculation is the input of the next calculation. The iteration continues until the diffraction screens out a self-reproductive mode, which is an optical field mode that can exist stably in a resonant cavity. That is, in the presence of a self-reproductive mode in the resonant cavity, the amplitude distribution of the optical field is fully reproducible if the beam diffracts and propagates in one round trip [24], [26]. As shown in Fig. 6(b), u_{q+1} can exactly reproduce the amplitude distribution of u_q when the resonant beam propagates enough times.

Afterwards, the beam energy in a plane is the integral of the beam power intensity concerning the plane area. The transmission loss is the difference between the energy on the two planes. Thus, after the resonant beam transmits from the transmitter to the receiver, the power transmission loss δ can be figured out as [27], [28]:

$$\delta = \frac{\iint_S |u_1|^2 \, ds - \iint_S |u_2|^2 \, ds}{\iint_S |u_1|^2 \, ds}. \tag{11}$$

C. Resonant Beam Output

According to the electromagnetic field propagation method, the beam power intensity at any position in the resonant cavity can be obtained and the beam transmission loss can be calculated by (10) and (11) accurately. The transmission coefficient (i.e.
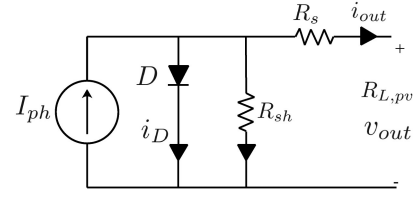

Fig. 7. Equivalent circuit of a photovoltaic panel.

transmission efficiency) ϵ of the resonant beam can be depicted as:

$$\epsilon = 1 - \delta. \tag{12}$$

We set the transmission coefficient from the transmitter to the receiver as ϵ_1, and the coefficient from the receiver to the transmitter as ϵ_2. Based on the above analysis, the formula of the output beam power P_{out} can be written as [18]:

$$P_{out} = A_b I_s \frac{(1-R)\epsilon_1}{1 - R\epsilon_1\epsilon_2 + \sqrt{R\epsilon_1\epsilon_2}(\frac{1}{\epsilon_1\epsilon_2 V_s} - V_s)} \left[g_0 \ell - \left| \ln \sqrt{R V_s^2 \epsilon_1 \epsilon_2} \right| \right], \tag{13}$$

where A_b is the cross-sectional area of the beam, I_s is the saturation intensity of the gain medium, R is the reflectivity of the output retro-reflector, V_s is the transmission coefficient in the gain medium. According to (1) and (2), if the excitation efficiency η_{excit} of the gain medium, whose value is decided by the medium's physical characteristics, is known, the small-signal gain can be calculated using:

$$g_0 \ell = \frac{\eta_{excit} P_{in}}{A I_s}, \tag{14}$$

where A is the cross-sectional area of the gain medium. Thus, (14) is substituted into (13) to obtain:

$$P_{out} = A_b I_s \frac{(1-R)\epsilon_1}{1 - R\epsilon_1\epsilon_2 + \sqrt{R\epsilon_1\epsilon_2}(\frac{1}{\epsilon_1\epsilon_2 V_s} - V_s)} \left[\frac{\eta_{excit} P_{in}}{A I_s} - \left| \ln \sqrt{R V_s^2 \epsilon_1 \epsilon_2} \right| \right]. \tag{15}$$

D. Energy Harvesting and Information Receiving

The output beam power is utilized to transfer energy and information. The power splitter in the receiver divides the received beam power into two power streams with a certain power-splitting ratio [5]. Let γ represent the power-splitting ratio. In addition, the energy stream is converted into electric power through the PV panel, and the information is received by the APD [29], [30].

D.1) Energy harvesting

Fig. 7 shows an equivalent circuit of the single-diode model for PV panel. Based on the general current-voltage characteristic of the PV panel, the output current i_{out} is:

$$i_{out} = I_{ph} - I_o \left[e^{\frac{v_{out} + i_{out} R_s}{n_s V_t}} - 1 \right] - \frac{v_{out} + i_{out} R_s}{R_{sh}}. \tag{16}$$

In the above equation, V_t is the junction thermal voltage:

$$V_t = \frac{FKT}{q}, \qquad (17)$$

where:

- I_{ph} - the photo-generated current
- I_o - dark saturation current
- R_s - panel series resistance
- R_{sh} - panel parallel (shunt) resistance
- F - diode quality (ideality) factor

are the parameters of the model, while K is the Boltzmann's constant, q is the quantity of electric charge, n_s is the number of cells in the panel connected in series, and T is the temperature in Kelvin. I_{ph} depends on the received beam power of PV panel, which can be expressed as

$$I_{ph} = \gamma \psi P_{out}, \qquad (18)$$

where ψ is the conversion responsivity of PV. Finally, the output electric power for energy supply can be written as:

$$P_e = i_{out} v_{out} = i_{out}^2 R_{L,pv}, \qquad (19)$$

where $R_{L,pv}$ is the load resistance of the PV panel.

D.2) Information Receiving

The maximum information transfer rate, i.e. spectral efficiency, can be written as [31]

$$C = \frac{1}{2} \log \left(1 + \frac{Se}{2\pi N} \right), \qquad (20)$$

where $\frac{S}{N}$ represents the signal-to-noise ratio (SNR). S is signal power and N is noise power. The signal power is [5], [31]

$$S = \left[(1 - \gamma) P_{out} \eta_{bi} \right]^2, \qquad (21)$$

where η_{bi} is the photo-electric conversion efficiency of APD. N is the power of an additive Gaussian white noise (AGWN), which can be expressed with shot noise N_{shot} and thermal noise $N_{thermal}$ as [5], [31]

$$\begin{aligned} N &= N_{shot}^2 + N_{thermal}^2 \\ &= 2q \left\{ \left[(1 - \gamma) P_{out} \eta_{bi} \right] + I_{bc} \right\} B_n + \frac{4KTB_n}{R_{L,apd}}, \end{aligned} \qquad (22)$$

where q is the quantity of electric charge, I_{bc} is the background current, B_n is the noise bandwidth, K is the Boltzmann's constant, T is the temperature in Kelvin, and $R_{L,apd}$ is the load resistor.

Furthermore, by varying the power-splitting ratio, the harvested energy and information rate can be balanced based on the system requirements. The end-to-end performance also can be improved by optimizing the transmission loss and the power-splitting ratio.

IV. NUMERICAL EVALUATION

In this section, to evaluate the SWIPT performance, we numerically analyze the transmission loss, output beam power, output electric power, spectral efficiency, and end-to-end efficiency of the RB-SWIPT system with specified structural parameters.

TABLE I
PARAMETERS RELATED TO THE GAIN MEDIUM, THE RETRO-REFLECTING
SURFACE AND FOX-LI ALGORITHM [18]

Symbol	Parameter	Value
I_s	Saturation intensity	$1260 W/cm^2$
V_s	Transfer coefficient of gain medium	99%
R	Output retro-reflector reflectivity	95%
η_{excit}	Excitation efficiency	51.48%
P_{in}	Input electric power	$200W$
N_{itr}	Fox-Li iteration number	300

TABLE II
PARAMETERS OF ENERGY HARVESTING [32]

Symbol	Parameter	Value
I_o	Dark saturation current	$9.89 \times 10^{-9} A$
F	Diode quality factor	1.105
n_s	Number of PV cell	40
R_s	Panel series resistance	0.93Ω
R_{sh}	Panel parallel resistance	$52.6k\Omega$
$R_{L,pv}$	Load resistance	100Ω
ψ	Conversion responsivity	$0.0161A/W$

TABLE III
PARAMETERS OF INFORMATION RECEIVING

Symbol	Parameter	Value
η_{bi}	Conversion efficiency of APD	$0.6A/W$ [34]
q	Quantity of electric charge	1.6×10^{-19}
B_n	Noise bandwidth	$811.7MHz$ [35]
I_{bc}	Background current	$5100\mu A$ [36]
K	Boltzmann constant	1.38×10^{-23}
T	Kelvin Temperature	$300K$
$R_{L,apd}$	Load resistor	$10K\Omega$ [37]

A. Parameter Setting

The parameters relevant to the numerical evaluation of SWIPT performance are shown in Table I, II and III [18], [33]. We adopt the thin crystal composed of Nd:YVO$_4$ as the gain medium, which is attached to the input retro-reflector and has the same radius as the retro-reflector [18]. The parameters related to the gain medium and the retro-reflector are presented in Table I. For energy harvesting, we adopt a vertical multi-junction PV cell. Table II shows the parameters of the PV panel, which are obtained by using PV equivalent circuit fitting measured data of a real PV cell product [32]. Meanwhile, as shown in Table III, we obtain parameters of APD according to experimental results using APD for information receiving [34], where q, K and T are generic. Besides, the parameters related to information receiving B_n, I_{bc}, and $R_{L,APD}$ are extracted from the corresponding literatures [35]–[37]. The power-splitting ratio γ can be determined based on the charging and communication needs.

B. Power Intensity Distribution in the Resonant Cavity

Using the Fresnel-Kirchoff's diffraction integral and "Fox-Li" numerical iteration method, the power intensity distribution in the RB-SWIPT system shown in Fig. 2 can be calculated. If the cavity length L is $1\,m$ and the radius of retro-reflector a is $1\,mm$, the power intensity distribution on the input retro-reflecting surface $S1$ is depicted in Fig. 8. The power intensity in the center of the surface is the largest, and it gradually decreases radially. Furthermore, the beam power intensity is equivalent at
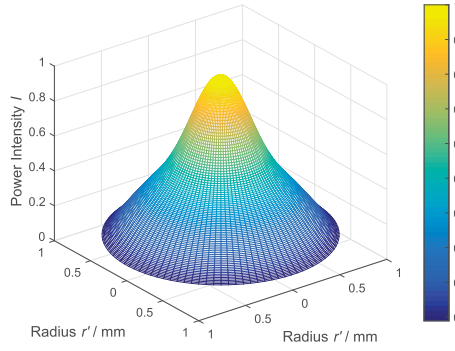
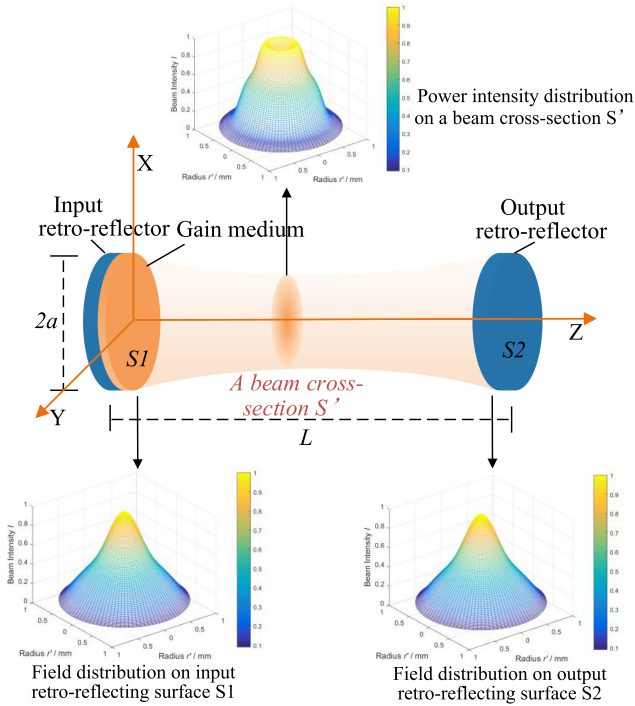Fig. 8.   Power intensity distribution on input retro-reflecting surface $S1$.

Fig. 10.   Transmission loss δ and output beam power P_{out} versus resonant cavity length L.

Fig. 9.   Power intensity at any position in the resonant cavity.

the same radial position on the retro-reflecting surface. When r' is 0.3 mm, the relative power intensity is about 0.7.

Afterwards, based on the calculation of Fresnel-Kirchoff's diffraction integral and "Fox-Li" numerical iteration, the beam power intensity of any position in the resonant cavity can be obtained, given the cavity length L and the retro-reflector radius a. As Fig. 9 shows, if the cavity length L is 1 m and the radius of retro-reflector a is 1 mm in an RB-SWIPT system, the resonant beam propagates as a Gaussian beam in the resonant cavity, and the power intensity distribution on any plane in parallel with the retro-reflecting surface (i.e. any beam cross-section) can be obtained. In Fig. 9, the power intensity distributions on input retro-reflecting surface $S1$, output retro-reflecting surface $S2$, and a beam cross-section S' are depicted. Afterwards, from the power intensity distributions, the power intensity of any point on $S1$, $S2$, and S' can be obtained. Similarly, the power intensity of any point in the resonant cavity can also be obtained through
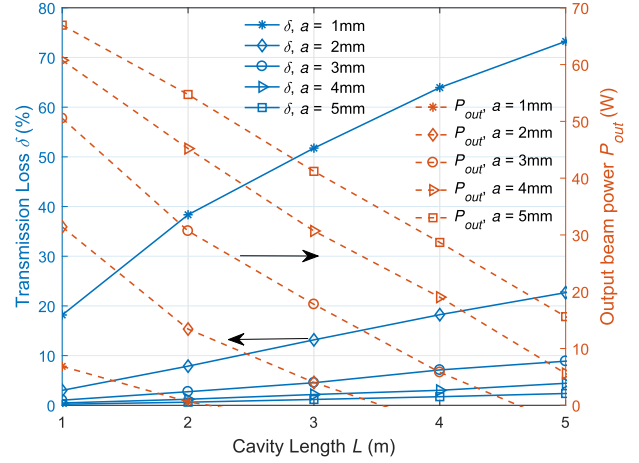
power intensity distribution on the plane parallel to the retro-reflecting surface. On this basis, the transmission loss in the cavity can be calculated in (11).

C. Transmission Loss and Output Beam Power

To evaluate the performance of RB-SWIPT system with different system structure parameters, we first analyze the transmission loss in the resonant cavity and the output beam power of the system under different cavity lengths and different radii of retro-reflectors.

The beam transmission loss from transmitter to receiver in the RB-SWIPT system can be figured out based on intra-cavity power intensity calculated by (3) and transmission loss in (11). The output beam power can be calculated based on (15). First of all, the transmission loss δ and output beam power P_{out} vary with cavity length L as depicted in Fig. 10. Since the beam power intensity decreases due to scattering and absorption inside the transmission medium, the transmission loss will increase with the increase of the transmission distance. As shown in Fig. 10, because of the increased influence of the transmission environment, increasing cavity length L leads that transmission loss δ amplifies under the radius of retro-reflector changing from 1 mm to 5 mm. That is, the growth of the transmission distance will increase the transmission loss in the resonant cavity. If the radius of retro-reflector is 5 mm and the cavity length is 1–5 m, the transmission loss is 0.21%, 0.62%, 1.17%, 1.72%, and 2.38%, respectively.

Conversely, due to the increased transmission loss, the output beam power P_{out} will decrease with the growth of cavity length L. As depicted in Fig. 10, P_{out} decreases as L increases with different retro-reflector radii. If P_{out} is less than 0 W, the pumping power at the transmitter does not reach the pumping threshold of the system, and there is no beam output. The output beam power is 66.94 W, 54.73 W, 41.20 W, 28.68 W, and 15.61 W respectively if the radius of retro-reflector is 5 mm and the cavity length is 1–5 m.
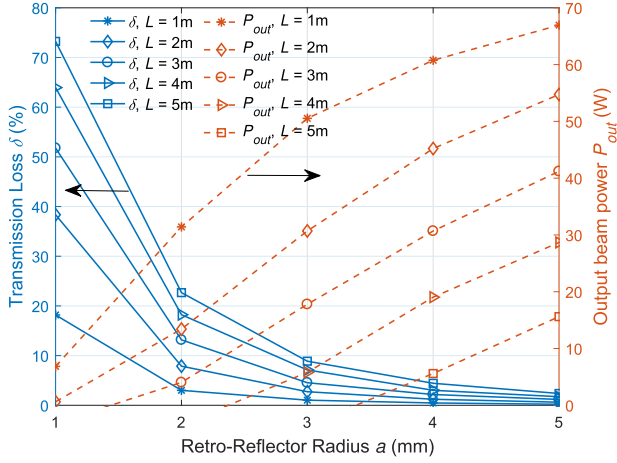
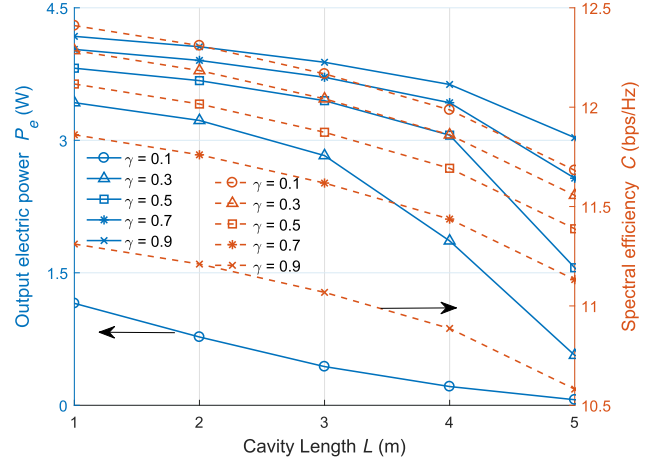Fig. 11. Transmission loss δ and output beam power P_{out} versus retro-reflector radius a.

Fig. 12. Output electric power P_e and spectral efficiency C versus resonant cavity length L.

Fig. 13. Output electric power P_e and spectral efficiency C versus retro-reflector radius a.

Furthermore, from Fig. 10, once the cavity length L is fixed, the transmission loss δ decreases and the output beam power P_{out} increases when using input and output retro-reflectors with larger radius. Fig. 11 depicts the change trends of transmission loss δ and output beam power P_{out} as the variation of the retro-reflector radius a.

In the resonant cavity, the resonant beam is paraxial distribution, i.e. the beam energy is concentrated towards the optical axis. In Fig. 11, since the power reception area increases, more resonant beam energy is stored in the cavity. Thus, the transmission loss δ decreases with retro-reflector radius a getting larger. If the cavity length is $3\,m$, the transmission loss δ is about 51.76%, 13.17%, 4.54%, 2.17%, and 1.17% respectively as the retro-reflector radius a increases from $1\,mm$ to $5\,mm$. Similarly, the output beam power P_{out} increases as a increases. If the cavity length is $1\,m$, the output beam power is $6.85\,W$, $31.42\,W$, $50.53\,W$, $60.76\,W$, and $66.94\,W$ as a is $1-5\,mm$.

D. Energy Harvesting and Information Receiving

According to (19) and (20), the output electric power and the spectral efficiency can be calculated when the retro-reflector size and the transmission distance are known. Thus, we analyze the output electric power P_e and the spectral efficiency C here with the changes of cavity length L and retro-reflector radius a under different power-splitting ratio γ.

According to above analysis, if the radius of the retro-reflector is $5\,mm$, we can obtain the maximum output beam power. Here, if a is $5\,mm$, we analyze the changes of output electric power P_e and the spectral efficiency C for power-splitting ratio γ as 0.1, 0.3, 0.5, 0.7 and 0.9 with the cavity length L as shown in Fig. 12. Based on (18) and (21), the output electric power P_e and spectral efficiency C are proportional to the output beam power P_{out}. As depicted in Fig. 12, since the output beam power decreases as the cavity length L extends, the output electric power P_e and spectral efficiency C decreases with the increase of L. For example, If γ is 0.3, P_e is about $3.43\,W$, $3.22\,W$, $2.83\,W$, $1.86\,W$, and $0.57\,W$, and C is $12.28\,bps/Hz$, $12.18\,bps/Hz$,
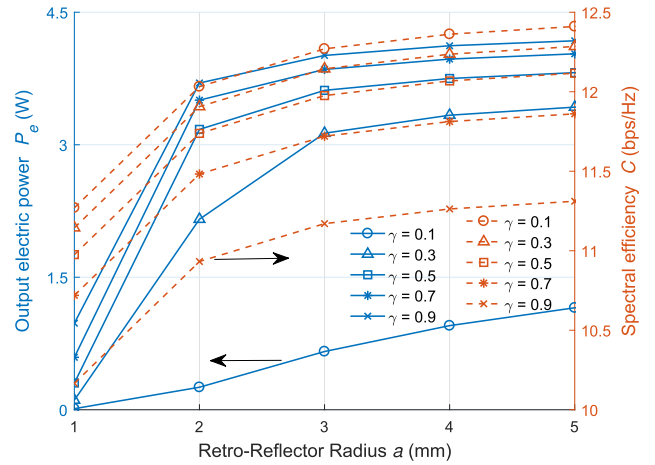
$12.04\,bps/Hz$, $11.86\,bps/Hz$, and $11.57\,bps/Hz$ respectively when L is $1-5\,m$.

In addition, if the cavity length L is $1\,m$, the maximum output beam power can be obtained in the RB-SWIPT system and the output beam power increases as the retro-reflector radius increases in Fig. 11. The change trends of the output electric power P_e and spectral efficiency C with the radius of retro-reflector a are demonstrated in Fig. 13. It can be seen from Fig. 13 that P_e and C increase when a gets larger independent of the power-splitting ratio γ. If γ is 0.3 and a increases from $1\,mm$ to $5\,mm$, the output electric power P_e is $0.10\,W$, $2.16\,W$, $3.13\,W$, $3.33\,W$, and $3.43\,W$, and spectral efficiency C is $11.14\,bps/Hz$, $11.91\,bps/Hz$, $12.14\,bps/Hz$, $12.24\,bps/Hz$, and $12.28\,bps/Hz$, respectively.

E. End-to-End Efficiency

To analyze the factors affecting the efficiency of the RB-SWIPT system, we study the changing trend of end-to-end efficiency as the cavity length and retro-reflector radius vary
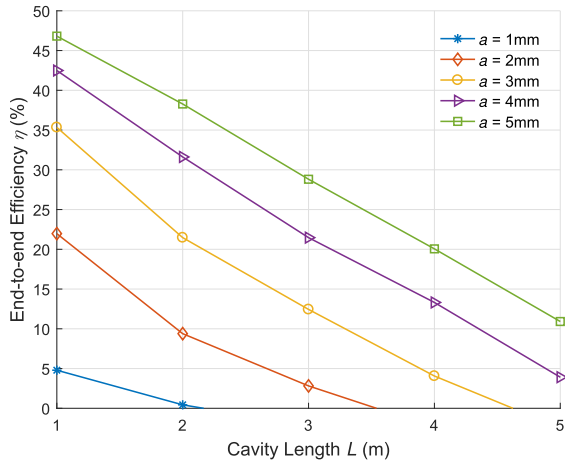
Fig. 14. End-to-end efficiency η versus cavity length L.

Fig. 15. End-to-end efficiency η versus retro-reflector radius a.

based on the above analysis of transmission loss, output beam power, output electric power, and spectral efficiency.

Under the premise that the output beam power P_{out} and the pumping optical power P_{gb} are known, the end-to-end efficiency η can be calculated using the ratio of P_{out} to P_{gb} (i.e. P_{out}/P_{gb}). According to [33], the electro-optical conversion efficiency is about 71.5%. Thus, P_{gb} is constant in an RB-SWIPT system with fixed input electric power. In this paper, we study the RB-SWIPT performance with $200\,W$ input electric power. Therefore, P_{gb} is about $143\,W$.

Since the output beam power P_{out} in Figs. 10 and 11 decreases with the extension of the cavity length L, the end-to-end efficiency η has the same trend as shown in Fig. 14. No matter how much the radius is, the end-to-end efficiency decreases with the increase of cavity length. If the retro-reflector radius is $5\,mm$, η is about 46.81%, 38.28%, 28.81%, 20.06%, and 10.92% as the cavity length L increases from $1\,m$ to $5\,m$.

In addition, as shown in Fig. 14, if the cavity length L is fixed, the end-to-end efficiency η increases as the radius of retro-reflector a magnifies because the output beam power P_{out} increases with the increase of retro-reflector radius a. The direct relationship between retro-reflector radius a and the end-to-end efficiency η can be obtained from Fig. 15. η has the same variation trend with P_{out} as the retro-reflector radius a changes. With the growth of the retro-reflector radius, the end-to-end efficiency rises regardless of the change of cavity length. That is, the larger radius a brings the smaller loss δ, leading to the greater output beam power P_{out}, and finally causes the higher end-to-end efficiency η. When L is $1\,m$, η is 4.79%, 21.97%, 35.34%, 42.49%, and 46.81% respectively as a is $1-5\,mm$.

F. Summary

Based on the E2E SWIPT model of the RB-SWIPT system, the power intensity in the resonant cavity can be calculated and analyzed. Then, the transmission loss increases with the cavity length extending and decreases with the retro-reflector radius getting larger. Afterwards, the output beam power, output electric power, and spectral efficiency in the receiver increase with the decrease of cavity length and increase of retro-reflector
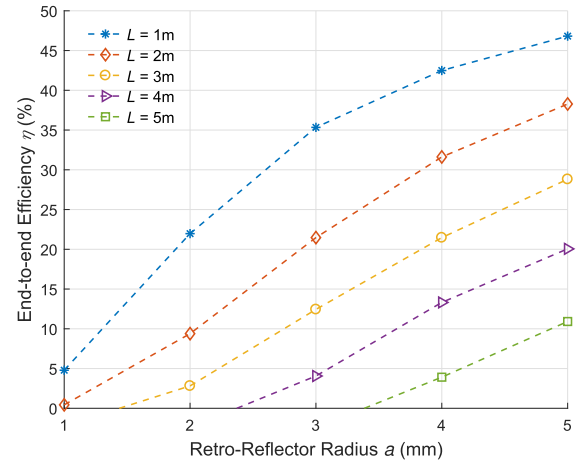
radius. Afterwards, the end-to-end charging efficiency and the output beam power have the same change trend with the change in cavity length and retro-reflector radius. Moreover, if the cavity length is $1\,m$ and the retro-reflector radius is $5\,mm$, the maximum output electric power is about $4.20\,W$ ($\gamma = 0.9$), and the maximum spectral efficiency is $12.41\,bps/Hz$ approximately ($\gamma = 0.1$). Finally, the end-to-end efficiency is 46.81% when the cavity length is $1\,m$ and the retro-reflector radius is $5\,mm$.

The requirements of energy supply and communication can be balanced by varying the power-splitting ratio. The operations to improve the E2E efficiency of the RB-SWIPT system include: i) designing a shorter resonant cavity (i.e. shorter transmission distance), and ii) using larger input/output retro-reflectors (i.e. a larger retro-reflector size).

V. CONCLUSIONS AND FUTURE WORK

The resonant beam simultaneous wireless information and power transfer (RB-SWIPT) system based on spatially separated laser-cavity is proposed in this paper. To reveal the energy-information transmission mechanism, we establish the end-to-end SWIPT model for calculating the intra-cavity power intensity, transmission loss, output electric power and spectral efficiency with different system parameters. Finally, the SWIPT performance is evaluated numerically with the $1-5\,m$ cavity length and $1-5\,mm$ retro-reflector radius. Numerical results illustrate that shorter transmission distance or larger retro-reflector sizes in both transmitter and receiver can improve the E2E efficiency for the RB-SWIPT system.

In the future research on the RB-SWIPT system, there are still many issues to be studied, for example:

i1) From electromagnetic field propagation for the RB-SWIPT system, the beam power intensity at any position in the resonant cavity can be obtained. Then, the safety of RB-SWIPT system can be analyzed based on the value of power intensity in the resonant cavity; and,

i2) The beam incident on a retro-reflector can be returned to the original path regardless of the angle of incidence. Afterwards, we can study the mobile energy transfer and communication using resonant beam.

REFERENCES

[1] Y. Chen, "Improved energy detector for random signals in Gaussian noise," *IEEE Trans. Wireless Commun.*, vol. 9, no. 2, pp. 558–563, Feb. 2010.

[2] I. Krikidis, S. Timotheou, S. Nikolaou, G. Zheng, D. W. K. Ng, and R. Schober, "Simultaneous wireless information and power transfer in modern communication systems," *IEEE Commun. Mag.*, vol. 52, no. 11, pp. 104–110, Nov. 2014.

[3] L. R. Varshney, "Transporting information and energy simultaneously," in *Proc. IEEE Int. Symp. Inf. Theory*, Toronto, Ontario, Canada, Jul. 6-11 2008, pp. 1612–1616.

[4] M. Agiwal, A. Roy, and N. Saxena, "Next generation 5G wireless networks: A comprehensive survey," *IEEE Commun. Surv. Tut.*, vol. 18, no. 3, pp. 1617–1655, Feb.

[5] T. D. P. Perera, D. N. K. Jayakody, S. K. Sharma, S. Chatzinotas, and J. Li, "Simultaneous wireless information and power transfer (SWIPT): Recent advances and future challenges," *IEEE Commun. Surv. Tut.*, vol. 20, no. 1, pp. 264–302, 2018.

[6] X. Liu, Q. Sun, W. Lu, C. Wu, and H. Ding, "Big-data-based intelligent spectrum sensing for heterogeneous spectrum communications in 5G," *IEEE Wireless Commun.*, vol. 27, no. 5, pp. 67–73, Oct. 2020.

[7] D. Masotti, M. Shanawani, G. Murtaza, G. Paolini, and A. Costanzo, "RF systems design for simultaneous wireless information and power transfer (SWIPT) in automation and transportation," *IEEE J. Microw.*, vol. 1, no. 1, pp. 164–175, Jan. 2021.

[8] W. Liu, X. Zhou, S. Durrani, and P. Popovski, "SWIPT with practical modulation and RF energy harvesting sensitivity," in *Proc. IEEE Int. Conf. Commun.*, Kuala Lumpur, Malaysia, May 23-27 2016, pp. 1–7.

[9] S. Ma, F. Zhang, H. Li, F. Zhou, Y. Wang, and S. Li, "Simultaneous lightwave information and power transfer in visible light communication systems," *IEEE Trans. Wireless Commun.*, vol. 18, no. 12, pp. 5818–5830, Dec. 2019.

[10] J. Fakidis, S. Videv, H. Helmers, and H. Haas, "0.5-Gb/s OFDM-based laser data and power transfer using a GaAs photovoltaic cell," *IEEE Photon. Technol. Lett.*, vol. 30, no. 9, pp. 841–844, May 2018.

[11] Q. Liu *et al.*, "Charging unplugged: Will distributed laser charging for mobile wireless power transfer work?," *IEEE Veh. Technol. Mag.*, vol. 11, no. 4, pp. 36–45, Dec. 2016.

[12] W. Fang, Q. Zhang, Q. Liu, J. Wu, and P. Xia, "Fair scheduling in resonant beam charging for IoT devices," *IEEE Internet Things J.*, vol. 6, no. 1, pp. 641–653, Feb. 2019.

[13] Q. Zhang, W. Fang, Q. Liu, J. Wu, P. Xia, and L. Yang, "Distributed laser charging: A wireless power transfer approach," *IEEE Internet Things J.*, vol. 5, no. 5, pp. 3853–3864, Oct. 2018.

[14] W. Wang, Q. Zhang, H. Li, M. Liu, X. Liao, and Q. Liu, "Wireless energy transmission channel modeling in resonant beam charging for IoT devices," *IEEE Internet Things J.*, vol. 6, no. 2, pp. 3976–3986, Apr. 2019.

[15] K. David and H. Berndt, "6G vision and requirements: Is there any need for beyond 5G?," *IEEE Veh. Technol. Mag.*, vol. 13, no. 3, pp. 72–80, Sep. 2018.

[16] M. Xiong, Q. Liu, G. Wang, G. B. Giannakis, and C. Huang, "Resonant beam communications: Principles and designs," *IEEE Commun. Mag.*, vol. 57, no. 10, pp. 34–39, Oct. 2019.

[17] W. Chen, S. Zhao, Q. Shi, and R. Zhang, "Resonant beam charging-powered UAV-assisted sensing data collection," *IEEE Trans. Veh. Technol.*, vol. 69, no. 1, pp. 1086–1090, Jan. 2020.

[18] N. Hodgson and H. Weber, *Laser Resonators and Beam Propagation: Fundamentals, Advanced Concepts, Applications*. Berlin, Germany: Springer, 2005.

[19] J. Lim, T. S. Khwaja, and J. Ha, "Wireless optical power transfer system by spatial wavelength division and distributed laser cavity resonance," *Opt. Exp.*, vol. 27, no. 12, pp. A924–A935, Jun. 2019.

[20] W. S. Rabinovich *et al.*, "Performance of cat's eye modulating retroreflectors for free-space optical communications," in *Proc. Free-Space Laser Commun. IV. Int. Soc. Opt. Photon.*, vol. 5550, Oct. 2004, pp. 104–114.

[21] J. Snyder, "Paraxial ray analysis of a cat's-eye retroreflector," *Appl. Opt.*, vol. 14, no. 8, pp. 1825–1828, Aug. 1975.

[22] J. Poirson, F. Bretenaker, M. Vallet, and A. Le Floch, "Analytical and experimental study of ringing effects in a fabry-perot cavity application to the measurement of high finesses," *J. Opt. Soc. Amer. B*, vol. 14, no. 11, pp. 2811–2817, Nov. 1997.

[23] S. Eftekharnejad, V. Vittal, G. T. Heydt, B. Keel, and J. Loehr, "Impact of increased penetration of photovoltaic generation on power systems," *IEEE Trans. Power Syst.*, vol. 28, no. 2, pp. 893–901, May 2013.

[24] A. Fox and T. Li, "Modes in a maser interferometer with curved and tilted mirrors," *Proc. IEEE*, vol. 51, no. 1, pp. 80–89, Jan. 1963.

[25] B. Lissak and S. Ruschin, "Transverse pattern modifications in a stable apertured laser resonator," *Appl. Opt.*, vol. 29, no. 6, pp. 767–771, Feb. 1990.

[26] A. G. Fox and T. Li, "Resonant modes in a maser interferometer," *Bell Syst. Tech. J.*, vol. 40, no. 2, pp. 453–488, Mar. 1961.

[27] J. Gordon and H. Kogelnik, "Equivalence relations among spherical mirror optical resonators," *Bell Syst. Tech. J.*, vol. 43, no. 6, pp. 2873–2886, Nov. 1964.

[28] T. Li, "Diffraction loss and selection of modes in maser resonators with circular mirrors," *Bell Syst. Tech. J.*, vol. 44, no. 5, pp. 917–932, May 1965.

[29] D. Sera, R. Teodorescu, and P. Rodriguez, "PV panel model based on datasheet values," in *Proc. IEEE Int. Symp. Ind. Electron.*, Vigo, Spain, 4-7 Jun. 2007, pp. 2392–2396.

[30] N. Cvijetic, S. G. Wilson, and M. Brandtpearce, "Performance bounds for free-space optical MIMO systems with APD receivers in atmospheric turbulence," *IEEE J. Sel. Areas Commun.*, vol. 26, no. 3, pp. 3–12, Apr. 2008.

[31] A. Lapidoth, S. M. Moser, and M. Wigger, "On the capacity of free-space optical intensity channels," *IEEE Trans. Inf. Theory*, vol. 55, no. 10, pp. 4449–4461, Nov. 2009.

[32] M. Perales *et al.*, "Characterization of high performance silicon-based VMJ PV cells for laser power transmission applications," in Proc. High-*Power Diode Laser Technol. Appl. XIV*, vol. 9733, Mar. 2016, Art. no. 97330U.

[33] P. Crump *et al.*, "100-W diode laser bars show $>71\%$ power conversion from 790- nm to 1000-nm and have clear route to $>85\%$," *Proc. SPIE*, vol. 6456, pp. 64560M.1–64560M.11, Feb. 2007.

[34] M. S. Demir, F. Miramirkhani, and M. Uysal, "Handover in VLC networks with coordinated multipoint transmission," in *Proc. IEEE Int. Black Sea Conf. Commun. Netw. (BlackSeaCom)*, Istanbul, Turkey, Jun. 5-8 2017, pp. 1–5.

[35] C. Quintana *et al.*, "High speed electro-absorption modulator for long range retroreflective free space optics," *IEEE Photon. Technol. Lett.*, vol. 29, no. 9, pp. 707–710, Mar. 2017.

[36] A. J. Moreira, R. T. Valadas, and A. de Oliveira Duarte, "Optical interference produced by artificial light," *Wireless Netw.*, vol. 3, no. 2, pp. 131–140, May 1997.

[37] F. Xu, M.-A. Khalighi, and S. Bourennane, "Impact of different noise sources on the performance of PIN-and APD-based FSO receivers," in *Proc. 11th Int. Conf. Telecommun.*, Graz, Austria, Jun. 15-17 2011, pp. 211–218.

Wen Fang received the B.E. degree in computer science and technology from the Shandong University of Science and Technology, Qingdao, China, in 2017. She is currently working toward the Ph.D. degree with the College of Electronics and Information Engineering, Tongji University, Shanghai, China.

Her research interests include wireless power transmission, development of remote wireless charging technology, and Internet of Things.

Hao Deng received the B.S. and Ph.D. degrees from the Department of Physical Electronics, University of Electronic Science & Technology, Chengdu, China, in 2007 and 2015, respectively. From 2017 to 2020, he was a Postdoctoral Research Fellow with the College of Electronics and Information Engineering, Tongji University, Shanghai, China. Since 2020, he has been a Lecturer with the School of Software Engineering, Tongji University. His research interests include optical critical dimension measurement for semiconductors, wireless power transfer, and Internet of Things.

Qingwen Liu (Senior Member, IEEE) received the B.S. degree in electrical engineering and information science from the University of Science and Technology of China, Hefei, China, in 2001, and the M.S. and Ph.D. degrees from the Department of Electrical and Computer Engineering, University of Minnesota, Minneapolis, MN, USA, in 2003 and 2006, respectively. He is currently a Professor with the College of Electronics and Information Engineering, Tongji University, Shanghai, China.

His research interests include wireless power transfer and Internet of Things.

Mingqing Liu received the B.S. degree in computer science and technology from Northwest A & F University, Yangling, China, in 2018. She is currently working toward the Ph.D. degree with the College of Electronics and Information Engineering, Tongji University, Shanghai, China.

Her research interests include wireless power transfer, development of remote wireless charging technology, and Internet of Things.

Mengyuan Xu received the B.E. degree in computer science and technology from the Jiangsu University of Science and Technology, Zhenjiang, China, in 2019. She is currently working toward the Ph.D. degree with the College of Electronics and Information Engineering, Tongji University, Shanghai, China.

Her research interests include wireless power transmission, development of remote wireless charging technology, and Internet of Things.

Liuqing Yang (Fellow, IEEE) received the Ph.D. degree in electrical and computer engineering from the University of Minnesota, Minneapolis, MN, USA, in 2004. She is currently a Professor with the University of Minnesota. She has authored or coauthored more than 330 journal and conference papers, four book chapters, and five books. Her general interests include communications and networking. She was the recipient of the ONR Young Investigator Program Award in 2007, and the NSF Faculty Early Career Development Award in 2009, the Best Paper Award at IEEE ICUWB'06, ICCC'13, ITSC'14, GLOBECOM'14, ICC'16, WCSP'16, GLOBECOM'18, ICCS'18, and ICC'19. She is the Editor-in-Chief of the *IET Communications*, an Executive Editorial Committee Member of the IEEE TRANSACTIONS ON COMMUNICATIONS, and the Senior Editor of the IEEE TRANSACTIONS ON SIGNAL PROCESSING. She was also the Editor of the IEEE TRANSACTIONS ON WIRELESS COMMUNICATIONS, IEEE TRANSACTIONS ON INTELLIGENT TRANSPORTATION SYSTEMS, IEEE INTELLIGENT SYSTEMS, and *PHYCOM: Physical Communication*, and the Program Chair, track or symposium or TPC Chair for many conferences.

Georgios B. Giannakis (Fellow, IEEE) received the Diploma degree in electrical engineering from the National Technical University of Athens, Athens, Greece, in 1981, and the M.Sc. degree in electrical engineering in 1983, the M.Sc. degree in mathematics, and the Ph.D. degree in electrical engineering from the University of the Southern California, Los Angeles, CA, USA, in 1983, 1986, and 1986, respectively. From 1982 to 1986, he was with the University of the Southern California.

From 1987 to 1998, he was with the University of Virginia, Charlottesville, VA, USA, and since 1999, he has been a Professor with the University of Minnesota, Minneapolis, MN, USA, where he holds an Endowed Chair of wireless telecommunications, University of Minnesota McKnight Presidential Chair of electrical and computer engineering, and the Director of the Digital Technology Center. He has authored or coauthored more than 450 journal papers, 750 conference papers, 25 book chapters, two edited books, and two research monographs (h-index 143) in his general interests, which include communications, networking, and statistical signal processing. His current research focuses on learning from big data, wireless cognitive radios, and network science with applications to social, brain, and power networks with renewables. He is the inventor or coinventor of 32 patents issued, and the recipient or co-recipient of nine best paper Awards from the IEEE Signal Processing (SP) and Communications (Com) Societies, including the G. Marconi Prize Paper Award in Wireless Communications. He was also the recipient of the Technical Achievement awards from the SP Society (2000), from the EURASIP (2005), the IEEE ComSoc Education Award (2019), the Young Faculty Teaching Award, the G. W. Taylor Award for Distinguished Research from the University of Minnesota, and the IEEE Fourier Technical Field Award (inaugural recipient in 2015). He is a Fellow of the EURASIP, and was the IEEE in a number of posts, including that of a Distinguished Lecturer for the IEEE-SP Society.